Available online at www.sciencedirect.com
ScienceDirect
Journal of Catalysis 244 (2006) 153–162
JOURNAL OF CATALYSIS
www.elsevier.com/locate/jcat

Structure and reactivity investigations on supported bimetallic Au–Ni catalysts used for hydrocarbon steam reforming

Ya-Huei (Cathy) Chin [1], David L. King *, Hyun-Seog Roh [2], Yong Wang, Steven M. Heald [3]

Institute for Interfacial Catalysis, Pacific Northwest National Laboratory, Richland, WA 99352, USA

Received 15 June 2006; revised 19 August 2006; accepted 21 August 2006

Available online 5 October 2006

Abstract

The addition of small quantities of gold to the surface of supported nickel catalysts has been described as a means to retard carbon formation during hydrocarbon steam reforming. Calculations by others have indicated that gold locates at the most catalytically active (step and edge) sites that also serve as nucleation sites for carbon formation. In this paper, we describe experiments to characterize the Ni–Au interactions on bimetallic Au–Ni/$MgAl_2O_4$ catalysts at various Ni and Au loadings. The catalyst structure was investigated using EXAFS/XANES spectroscopy and adsorption–desorption measurements with H_2 and N_2O. Evidence for surface alloy formation is provided in the Ni K-edge and Au L_{III}-edge EXAFS measurements of Au-promoted 8.8% Ni/$MgAl_2O_4$, especially at Au loadings $\leqslant$0.2 wt%. At higher Au concentrations, there is evidence of a combination of alloy and segregated Au species. H_2 chemisorption and N_2O temperature-programmed desorption (TPD) measurements showed a significant decrease in total surface sites, or surface site reactivity, on Au-modified Ni/$MgAl_2O_4$ catalyst. The XANES structure is consistent with perturbation of the electronic structure of both the Ni and Au atoms as a result of alloy formation. TGA studies with steam/*n*-butane feed confirmed the ability of Au to retard coke deposition under low S/C reforming conditions, although carbon formation was not fully suppressed. When testing for methane steam reforming, a lower initial activity and deactivation rate resulted from Au promotion of the Ni catalyst. However, both catalysts showed a declining activity with time. The lack of a direct correlation between the surface characterization results and catalytic activity is most likely a result of decreasing effectiveness of the surface alloy with increasing temperature.

Keywords: EXAFS; XANES; Steam reforming; Nickel; Ni; Gold; Au; Bimetallic; Surface alloy; N_2O decomposition

1. Introduction

Catalytic steam reforming of light hydrocarbons to produce hydrogen is of significant industrial importance [1–3] and is of increasing interest in the context of a "hydrogen economy." Commercial steam-reforming processes use Ni-based catalysts because of their acceptably high activity and significantly lower cost in comparison with alternative precious metal-based catalysts. However, nickel-based catalysts are susceptible to deactivation from the deposition of carbon [4], even when operating at steam-to-carbon ratios predicted to be thermodynamically outside of the carbon-forming regime [5]. Both reforming and coke deposition are believed to be initiated by the same elementary hydrocarbon activation step [6]. Under steam-reforming conditions, metal surfaces are covered with various CH_x intermediates. Without a fast steam gasification step to convert these intermediates to CO and H_2, these adsorbed CH_x species on Ni surface can undergo further dehydrogenation, polymerization, and rearrangement into highly stable carbon species [7]. These stable carbon species not only show low reactivity toward the gasification reaction, but also may dissolve into or encapsulate the Ni particles. In some cases, the dissolution leads to whisker carbon growth that eventually destroys the catalyst and plugs the reactor.

* Corresponding author. Fax: +1 509 375 3908.
E-mail address: david.king@pnl.gov (D.L. King).
[1] Current address: Department of Chemical Engineering, University of California, Berkeley, CA 94720, USA.
[2] Current address: Korea Institute of Energy Research, 71-2, Jang-dong, Yuseong-gu, Daejeon 305-343, South Korea.
[3] Current address: Advanced Photon Source, Argonne National Laboratory, Argonne, IL 60439, USA.

0021-9517/$ – see front matter
doi:10.1016/j.jcat.2006.08.016

For methane steam reforming, mechanistic and molecular-level reaction pathway studies show that dissociative adsorption of the H_3C–H bond to form adsorbed –CH_3 and –H is the kinetically rate-determining step. This rate was confirmed by Wei and Iglesia [8] through kinetic dynamic and isotopic investigations of Ni/MgO catalysts for methane decomposition and for methane reforming by CO_2 and H_2O. Density functional theory (DFT) calculations indicate significant differences in reactivity of the various exposed Ni crystallographic planes toward activating methane. For example, a coordinatively unsaturated surface such as a Ni(211) plane, which tends to be prevalent in smaller metal clusters, exhibited higher reactivity toward C–H bond activation than the planar Ni(111) surface, with an activation energy difference of the first C–H bond breaking in CH_4 of approximately 20 kJ/mol [6]. However, such sites are also more likely to facilitate carbon nucleation. It is postulated that the nucleated carbon species on the stepped sites grow to stable graphene-type moieties. It follows that loss of catalyst activity due to carbon deposition can be minimized by inhibiting carbon nucleation. Selective poisoning of the high-activity sites provides one method to retard carbon deposition and is commercially practiced. In the Sparg process, trace quantities of hydrogen sulfide are introduced continuously into a commercial reformer [9,10] to control carbon formation. Sulfur is thought to preferentially adsorb on the more reactive Ni sites, poisoning those sites and retarding carbon nucleation at the expense of some loss of activity [11].

Extending this concept, reactivity and deactivation by carbon formation can also in principle be controlled by modifying Ni surfaces with a second metal, such as gold, through alloy formation. Due to a large miscibility gap, binary Ni and Au systems do not form a bulk alloy over the entire concentration range [12]; rather, a surface alloy forms. It is possible for gold to locate at planar sites, resulting in smaller Ni ensembles, at the high-energy step, edge sites, or both. A STM study of Au deposited on Ni(110) by Pleth Nielsen et al. [13] provided experimental evidence of Ni–Au alloy formation on the surface of a Ni single crystal. In contrast, Monte Carlo simulations on a nanocluster with random initial Ni and Au atom distribution showed the selective outward migration of Au to form a stable surface alloy, with the Au located preferentially at the high-energy step and edge sites [6]. The pathfinding catalytic work by Besenbacher et al. [14] on Ni–Au showed that an Au-promoted Ni/$MgAl_2O_4$ catalyst is less susceptible to carbon formation during *n*-butane reforming at 550 °C and low S/C ratios. However, the loss of activity as a result of Au promotion, as well as the effect of Au addition on steam reforming under conditions more typical of industrial reformer operation, was not described.

In the course of investigating the Au–Ni/$MgAl_2O_4$ catalyst system for steam reforming, we became interested in a more detailed characterization of its surface properties. This study provides data characterizing the surface properties of Ni/$MgAl_2O_4$ catalysts modified by Au, prepared via impregnation, using EXAFS (extended X-ray absorption fine structure), XANES (X-ray absorption near-edge spectroscopy), N_2O TPD (temperature-programmed desorption), and H_2 chemisorption. We also provide thermogravimetric data from *n*-butane steam reforming and catalytic data from methane steam reforming, to correlate the results of the surface characterization with catalytic performance.

2. Experimental

2.1. Catalyst synthesis

Two Ni/$MgAl_2O_4$ catalyst batches with 8.8 and 15.8 wt% Ni content were prepared by the incipient wetness impregnation method. $MgAl_2O_4$ (Sasol, 30 wt% MgO, 146 m^2/g) was calcined at 700 °C in air for 3 h, followed by impregnation with nickel nitrate ($Ni(NO_3)_2{\cdot}6H_2O$, Aldrich 99%). The sample was then calcined at 500 °C in air for 4 h. For bimetallic Au–Ni/$MgAl_2O_4$ catalysts, Au was added by incipient wetness impregnation with aqueous hydrogen tetrachloroaurate(III) hydrate (Aldrich, 99.999%) onto previously reduced and passivated Ni/$MgAl_2O_4$. Reduction and passivation of the Ni/$MgAl_2O_4$ catalyst involved reducing the sample to H_2 at 700 °C for 2 h, followed by cooling to room temperature under He, then exposing the sample to 1% O_2/He overnight. After being impregnated with Au, the sample was dried in ambient air, heated in flowing He at a rate of 1 °C/min to 200 °C, then held isothermally at 200 °C for at least 8 h.

2.2. Catalyst characterization

H_2 volumetric chemisorption and N_2O TPD were measured using a RXM-100 advanced catalyst characterization system. A 250-mg catalyst sample was loaded into a quartz holder and reduced using a temperature ramp and soak program: ambient to the reduction temperature at 5 °C/min followed by 2 h isothermal hold at the reduction temperature. The sample was then evacuated for 30 min under high vacuum before cooling to room temperature. H_2 chemisorption was conducted at room temperature in a static volumetric adsorption mode, with a H/Ni stoichiometry of 1 assumed. N_2O TPD was performed by exposing the sample to 90 Torr N_2O for 30 min at ambient temperature, evacuating for 30 min, and then heating at a constant ramp rate of 8 °C/min to 900 °C under vacuum. Desorbed species were monitored by a quadrupole mass spectrometer.

Ni K-edge and Au L_{III}-edge EXAFS and XANES experiments were performed at the PNC-XOR beamline at the Advanced Photon Source at Argonne National Laboratory. The station was equipped with a Si(111) double-crystal monochromator. Fluorescent radiation was collected using a DXP detector. Catalyst samples were pretreated and mounted onto self-supporting wafers in a Displex chamber under controlled atmosphere. The cell was cooled to below 50 K before absorption data were collected for EXAFS and XANES in the fluorescent mode. Extraction of the EXAFS data from the measured fluorescence was performed with University of Washington analysis programs. The raw data were smoothed, background-corrected, normalized, and fitted at a *k* range of 2–13.65 using the first shell theoretical scattering amplitudes and phase shifts

of Au–Ni, and Au–Au calculated from the FEFF7 code. Interatomic distances of 2.884 and 2.688 Å were used to generate the theoretical scattering amplitudes and phase shifts for Au–Au and Au–Ni, respectively.

2.3. Thermogravimetric measurements

Coke deposition from *n*-butane steam reforming was measured on a Netzsch STA409 microbalance at a S/C ratio of 0.7. The samples were prereduced ex situ at 900 °C under H_2 and passivated at room temperature in 1% O_2. Before the sample was exposed to steam-reforming conditions, it was rereduced in situ at 600 °C for 4 h and cooled to 300 °C in 2% H_2/Ar. A stream comprising 2.1% of steam and 0.75% *n*-butane (balance He) was introduced at 300 °C, and the sample was subsequently heated to the selected reaction temperature at 10 °C/min and held isothermally at the reaction temperature.

2.4. Catalyst activity testing

Methane steam-reforming activity was measured at 550 °C at a steam-to-carbon ratio of 1, using a feed comprising 45% CH_4, 45% H_2O, and 10% H_2. The catalysts were diluted with $MgAl_2O_4$ at a ratio of 1/19 and pelletized to 60–100 mesh. The pelletized powder was then rediluted with $MgAl_2O_4$ of the same mesh size at a ratio of 2/13 and loaded in a microcatalytic fixed-bed quartz reactor. Before testing, the catalysts were reduced in situ for 2 h at 700 °C.

3. Results

3.1. H_2 chemisorption studies

A preliminary TPR experiment was performed to determine the role of reduction temperature on the extent of Ni metal reduction. This is shown in Fig. 1 for 15.8% Ni/$MgAl_2O_4$ using 8% H_2/Ar as the reducing gas. The reduction initiated at 475 °C and reached completion by 900 °C. Reduction at 900 °C with dilute H_2 yielded catalysts having the highest hydrogen uptake for both the 8.8 and 15.8% Ni samples. This is shown in Table 1 for the 8.8% Ni/$MgAl_2O_4$ catalyst. The reference sample, $MgAl_2O_4$ support without Ni, adsorbed a negligible amount of H_2. Because the apparent increase in dispersion from 7.1 to 7.9% with increasing reduction temperature is due to the increasing fraction of Ni reduced (Fig. 1), the hydrogen uptake and dispersion values are more meaningful than the calculated crystallite size.

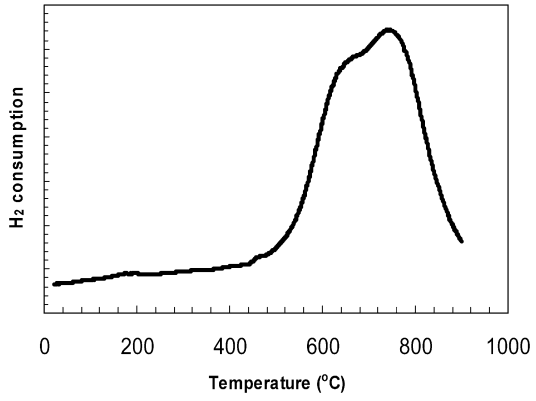

Fig. 1. H_2 consumption during TPR of 15.8% Ni/$MgAl_2O_4$ with 8% H_2/92% Ar at a ramp rate of 8 °C/min.

Table 1
Variation in H_2 chemisorption with reduction conditions for 8.8 wt% Ni/$MgAl_2O_4$

Reduction temperature (°C)	Reduction gas composition	H_2 uptake (μmol H_2/g_{cat})	Equivalent dispersion (%)	Calculated crystallite size (nm)
700	8% H_2–92% Ar	53.5	7.1	10.1
800	8% H_2–92% Ar	56.8	7.6	9.6
900	8% H_2–92% Ar	59.1	7.9	9.2
900	100% H_2	49.3	6.6	11.0

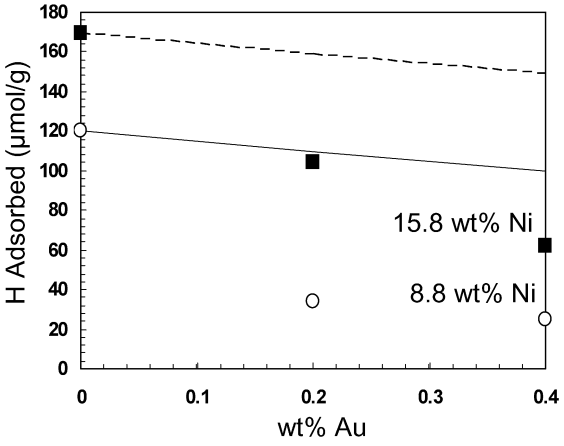

Fig. 2. H_2 chemisorption of Au-promoted Ni/$MgAl_2O_4$ catalysts after reduction in 8% H_2/92% Ar at 900 °C for 2 h: (■) 15.8 wt% Ni; (○) 8.8 wt% Ni. The lines represent the calculated reduction in H_2 adsorption due to physical site blockage of Au atoms on the Ni surface.

Fig. 2 shows the H_2 chemisorption results obtained with the 8.8 and 15.8% Ni/$MgAl_2O_4$ catalysts to which gold was added at two different loadings after reduction at 900 °C. For comparison purposes, the reduction in hydrogen uptake that would result from physical site blockage caused by Au atop a single Ni site is calculated and plotted in the same figure for both catalysts. Addition of Au significantly reduced the total amount of H_2 chemisorbed on the catalysts. With the 15.8% Ni catalyst, addition of 0.2% Au reduced H_2 chemisorption from 169 to 104 μmol H/g_{cat}. This is a decrease on a per-gram of catalyst basis of 65 μmol H caused by 10 μmol of Au, indicating an Au effect extending beyond simple site blockage. The effect of Au was even greater for the 8.8% Ni sample, where the same 10 μmol of Au (0.2 wt%) caused a decrease of approximately 85 μmol H. Increasing the Au concentration to 0.4% resulted in further suppression of the amount of H_2 adsorbed. Suppression of H_2 uptake was also reported by Yuan et al. [15] in a recent study of a Ni–Au/SiO_2 catalyst. Such results suggest a significant decrease in surface sites or surface reactivity after addition of Au.

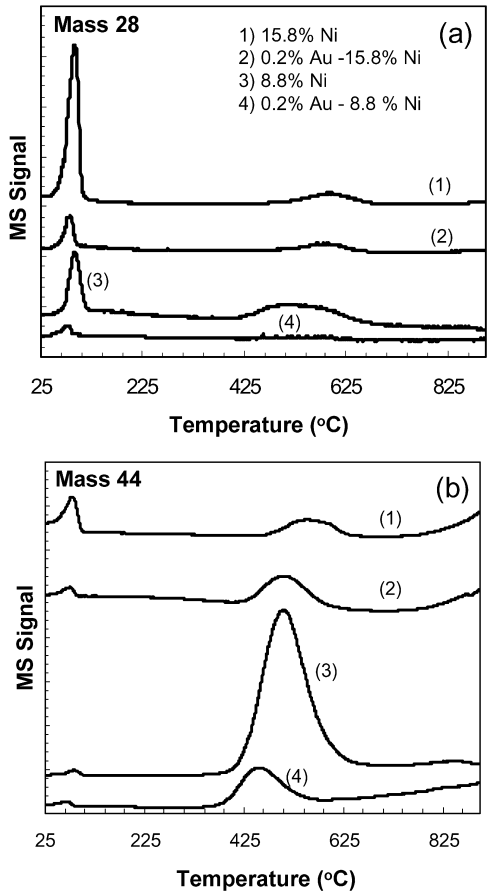

Fig. 3. Desorption of mass 28 (a) and 44 (b) during N_2O TPD over Au-promoted Ni/$MgAl_2O_4$ catalysts. Catalyst were prereduced in situ prior to N_2O adsorption to 900 °C for 2 h under 8% H_2/92% Ar.

3.2. N_2O TPD as a probe reaction for surface reactivity

Ni catalysts have recently been found to be active for direct N_2O decomposition at low temperatures [16,17]. In our experiments, N_2O TPD was carried out by exposing the catalyst sample to 90 Torr N_2O at room temperature for 30 min, followed by evacuation and then heating at 8 °C/min under high vacuum. During the TPD measurements, N_2 and N_2O were detected as the primary desorbing species. Desorption profiles are presented in Figs. 3a and 3b for masses 28 and 44, respectively. Two distinct desorption features are seen: (1) a low-temperature desorption of mass 28 that can be assigned to molecular N_2 and (2) a high-temperature desorption of mass 44 assigned to molecular N_2O.

On the unpromoted Ni/$MgAl_2O_4$ samples [traces (1) and (3)], significant desorption of N_2 was observed at low temperatures, with desorption completed below 130 °C. Desorption profiles for O_2 at mass 16 and mass 32 were monitored during the TPD experiment, but no evidence of O_2 evolution was observed below 300 °C. Although our best estimates are that the total number of sites that generate N_2 (and NiO) from N_2O are roughly similar in quantity to the sites detected by H_2 chemisorption, accurately quantifying these results is difficult, because some weakly held N_2 may have escaped undetected during the evacuation step before initiation of the TPD measurements.

High-temperature N_2O desorption occurred over these same samples from approximately 400 to 625 °C. N_2O TPD was also performed over a bare $MgAl_2O_4$ reference sample (not shown). That sample showed desorption of mass 44 below 150 °C, but no signal at mass 28 was observed. A small N_2O desorption peak at higher temperatures was also detected.

From the TPD profile, it can be concluded that N_2O is chemisorbed both dissociatively and associatively on Ni surfaces, along with being physisorbed by the $MgAl_2O_4$ support. Metallic Ni surfaces dissociatively chemisorb N_2O, oxidizing Ni to NiO with co-production of molecular N_2 just above room temperature. This is evidenced by the desorption of mass 28 at low temperature and the lack of detectable O_2 evolution. Desorption of N_2O at high temperature indicates the presence of strongly chemisorbed N_2O wherein the N–O bond is not activated to undergo dissociation. Quantitative analysis of the N_2 evolution profile shows a disproportionately higher quantity of N_2 evolved from the 15.8% Ni catalyst in comparison with the 8.8% Ni sample. In contrast, desorption of molecular N_2O was significantly lower from the 15.8% Ni catalyst. The evolution of mass 28 at high temperatures is not related to N_2 evolution, but is an artifact arising from mass fragmentation of N_2O.

Promoting Ni/$MgAl_2O_4$ with 0.2% Au modified the N_2O TPD profile for both the 8.8 and 15.8% Ni samples. The low-temperature N_2 peaks of the Au-free catalysts were significantly suppressed over both samples after promotion by Au. Comparing Figs. 2 and 3a indicates that Au promotion suppressed the reaction with N_2O to produce N_2 and NiO to an even greater extent than chemisorption of H_2. Again, this suggests a significant loss of surface reactivity after addition of Au. The high-temperature mass 44 peak from the 8.8% Ni sample was also substantially decreased after the addition of 0.2% Au, and the peak maximum decreased. A similar decrease in the high-temperature mass 44 peak was not observed with the 15.8% Ni sample after addition of Au, but a decrease in the peak maximum was evident, analogous to the 8.8% Ni sample.

3.3. EXAFS measurements

Fig. 4a shows the radial distribution function obtained from Au L_{III}-edge EXAFS measurements of a nickel-free Au/$MgAl_2O_4$ sample after reduction or after oxidation at 500 °C. This figure also plots the radial distribution function of an oxidized 0.2% Au–8.8% Ni/$MgAl_2O_4$ sample. Little difference is seen in these three spectra. The Au EXAFS data were fitted with phase and amplitude functions derived from the first three shells of Au–Au interaction, shown in Fig. 4b. Metallic Au clusters were present on both the monometallic Au and the Au–Ni samples after the oxidative treatment at 500 °C. Fitting the EXAFS data indicates an average first-shell coordination number $N_{Au–Au} > 11$, as shown in Table 2. These results suggest that the only detectable gold species in these samples were clusters of zerovalent Au atoms. There is no indication of significant interaction between gold and nickel after oxidative treatment.

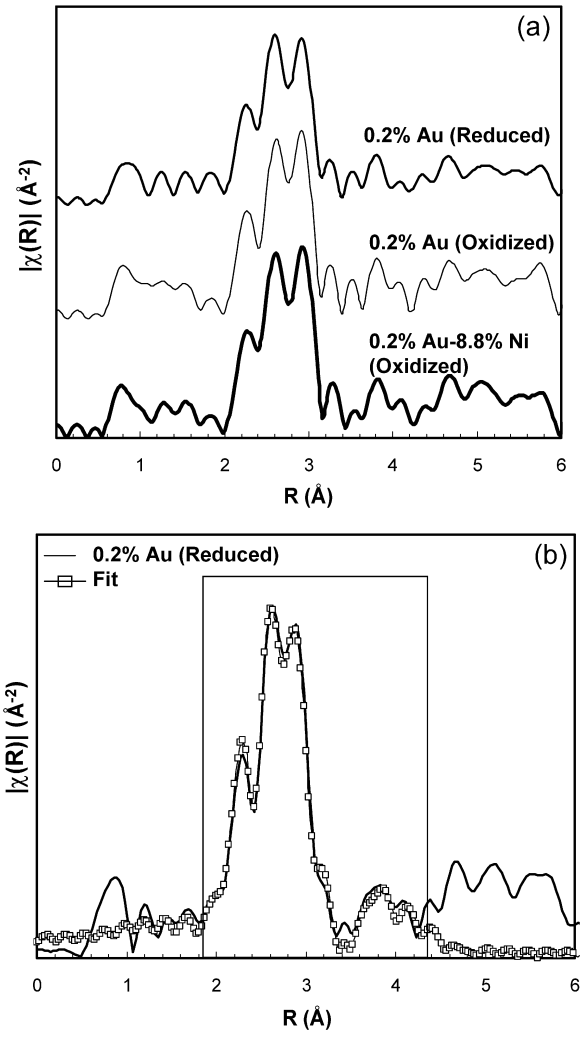

Fig. 4. (a) k^1-weighted Fourier transform of Au L_{III}-edge EXAFS for Au–Ni and Au supported on $MgAl_2O_4$ after reduction or oxidation at 500 °C. (b) Comparison of the Fourier-transformed EXAFS data of 0.2% Au/$MgAl_2O_4$ with fitting the first three shells of Au–Au interactions in a fcc structure.

The Au–Ni interaction was then probed by Ni K-edge and Au L_{III}-edge EXAFS on a series of reduced Au–8.8% Ni/$MgAl_2O_4$ catalysts containing varying gold concentrations. As mentioned previously, these catalysts were prereduced to 700 °C during synthesis before the Au promoters were incorporated. After the Au precursor was added, the catalysts were reduced again at 500 °C before the EXAFS measurements. No significant difference was detected in Ni K-edge EXAFS over the entire series of samples (not shown). Only contributions from Ni–Ni interaction were observed; there was no evidence of Ni–Au contribution to the Ni K-edge EXAFS. This is most likely due to the very high concentration of Ni relative to Au in these samples.

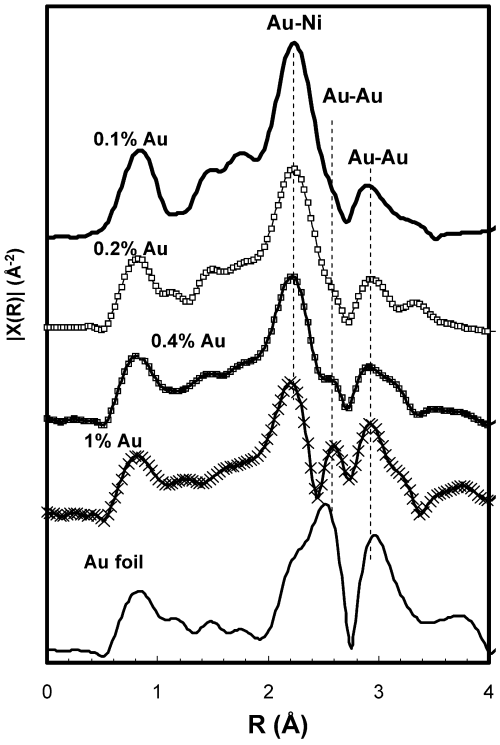

Fig. 5. k^1-weighted Fourier transform of Au L_{III}-edge EXAFS for Au–8.8% Ni/$MgAl_2O_4$ after reduction at 500 °C. A spectrum of Au foil EXAFS is included as reference. Contribution of Au–Ni and Au–Au interactions are labeled in the corresponding regions.

However, the EXAFS data obtained at the Au L_{III} edge revealed significant changes to the Au local structure in the presence of Ni. This is shown in Fig. 5, which provides the k^1-weighted Fourier transforms of the EXAFS spectra. In addition to small contributions from Au–Au interactions, a new feature was detected at 2–2.5 Å (not phase-corrected). Features in this region were previously ascribed to Au–Ni hetero-atomic bonding in the first coordination shell, further confirmed by ab initio calculated EXAFS signals based on an Au–Ni theoretical model using FEFF 8.00 code [18]. The EXAFS data from the low-loading Au sample (0.1%) showed primarily an Au–Ni contribution and a negligible Au–Au contribution. With increasing Au loading, the data revealed an increase in Au–Au interactions. Table 3 shows the result of fitting the back-transformed Au L_{III}-edge data with both the Au–Ni and Au–Au first coordination shells. On the sample with the lowest Au loading (0.1% Au), the average Au–Ni coordination number was 5.3, with a negligible coordination number of Au–Au interaction.

Table 2
Structural parameters derived from fitting Au L_{III}-edge EXAFS data for Au/$MgAl_2O_4$ following either oxidation or reduction, and for Au–Ni/$MgAl_2O_4$ after oxidation, all at 500 °C

Catalyst	Pretreatment	N	R (Å)	$\Delta\sigma^2 \times 10^3$	ΔE_0	R factor (%)
0.2% Au/MgO–Al_2O_3	Reduced at 500 °C	11.3 ± 0.6	2.86 ± 0.002	2.4 ± 0.3	5.62	0.4
0.2% Au/MgO–Al_2O_3	Oxidized at 500 °C	11.0 ± 0.6	2.86 ± 0.002	1.9 ± 0.3	5.62	0.4
0.2% Au–8.8% Ni/MgO–Al_2O_3	Oxidized at 500 °C	11.9 ± 0.9	2.87 ± 0.003	2.0 ± 0.4	4.89	1.0

Table 3
Structural parameters derived from fitting Au L_{III}-edge EXAFS data for Au–8.8% Ni/$MgAl_2O_4$ after reduction at 500 °C

Au concentration (%)	Au L_{III}-edge fitting Au–Ni				Au L_{III}-edge fitting Au–Au				*R* factor (%)
	N	*R* (Å)	$\Delta\sigma^2 \times 10^3$	ΔE_0	*N*	*R* (Å)	$\Delta\sigma^2 \times 10^3$	ΔE_0	
0.1	5.3 ± 1.1	2.58 ± 0.01	6.5 ± 1.6	0.2	–	–	–	–	4.7
0.2	4.9 ± 1.1	2.59 ± 0.02	7.4 ± 1.6	4.2	4.0 ± 1.3	2.97 ± 0.04	8.3 ± 4.3	5.4	4.9
0.4	3.7 ± 0.7	2.58 ± 0.01	5.5 ± 0.1	2.8	6.0 ± 1.5	2.82 ± 0.01	7.7 ± 1.8	4.9	2.1
1.0	2.8 ± 0.3	2.57 ± 0.01	4.3 ± 0.7	4.1	7.6 ± 1.0	2.84 ± 0.01	6.5 ± 0.6	6.3	4.7

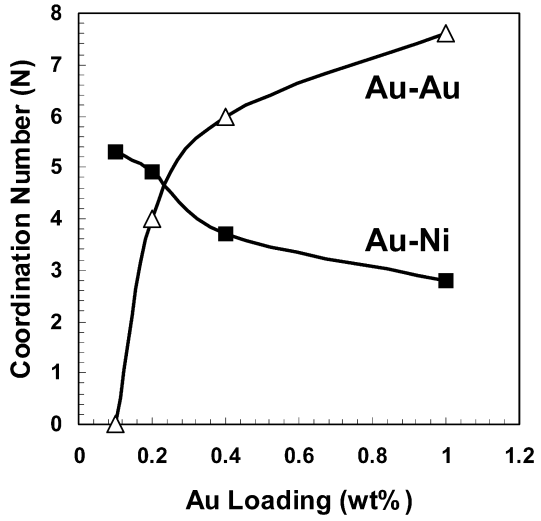

Fig. 6. Au–Au and Au–Ni interaction after reduction of Au–8.8% Ni/$MgAl_2O_4$ catalyst at 500 °C. The average Au–Au (△) and Au–Ni (■) coordination numbers are derived from fitting the Au L_{III}-edge EXAFS data of Au–8.8% Ni/$MgAl_2O_4$.

On this sample, essentially all of the Au atoms were bonded to Ni as the next nearest neighbor. Increasing Au loadings resulted in increased Au–Au interaction and a parallel decrease in Au–Ni interaction. This is evident in the Fourier transform of the EXAFS data in Fig. 5, and the relationship of N_{Au-Au} and N_{Au-Ni} with Au loading is further illustrated in Fig. 6. For the 1% Au–8.8% Ni sample, an increase in Au–Au interaction was evident with an average Au–Au coordination of 7.6.

3.4. Ni K-edge and Au L_{III}-edge XANES

The XANES regions for both the Ni K and Au L_{III} edges showed significant modifications as a result of Au–Ni interactions. Fig. 7 plots Ni K-edge XANES spectra over a series of reduced 8% Ni/$MgAl_2O_4$ samples with different Au loadings, along with a Ni foil reference. As shown, the gold-free Ni catalyst exhibited white line intensity between the Ni foil reference and the same catalyst after oxidation at 500 °C. This is not surprising, because the XANES spectrum is a weighted sum of the overall Ni environment in the entire sample. Based on the TPR and chemisorption results described above, it is possible that some of the Ni on the catalyst is not fully reduced after treatment in H_2 at 700 °C, and a small fraction of Ni is most likely present in a higher oxidation state as either NiO or in a spinel structure. Adding Au to the Ni catalyst resulted in modification of the Ni K-edge XANES spectrum. The white line intensity generally was increasingly suppressed with increasing Au concentration, although the 0.1% Au sample demonstrated the greatest effect. These results imply that the Ni atoms are on average more reduced when interacting with Au.

For the Au L_{III}-edge XANES, reduced monometallic Au/$MgAl_2O_4$ exhibited XANES structures similar to those of the Au foil (Fig. 8). The XANES spectrum of the 0.2% Au–8.8% Ni/$MgAl_2O_4$ sample, after oxidation at 500 °C, also had the same profile (not shown) with the spectrum taken on Au foil. From both XANES and EXAFS results, it can be concluded that the oxidation state of gold remained as Au^0 in both reducing and oxidizing environments. This is not an unexpected result, even after high-temperature oxidation of the Au–Ni catalyst, because Au_2O_3 is not a thermodynamically stable phase under these conditions [19].

More interestingly, the entire Au L_{III}-edge XANES structure changed with the presence of Ni. The XANES spectra on the same series of samples all showed increased white line intensity. Closer examination of the spectra (Fig. 8) revealed that the 0.1% Au–Ni sample exhibited the greatest white line intensity, and that white line intensity decreased with increasing Au loading. Increased white line intensity points toward a shift in electron density from the Au atoms on interaction with Ni. Modifications in both the Ni K and Au L_{III} XANES spectra suggest significant interaction between the Ni and Au atoms. As a result, the oxidation states of Ni and Au are modified (Ni more electron-rich, Au more electron-poor) compared with the pure monometallic samples.

3.5. Thermogravimetric analysis of coke deposition during *n*-butane steam reforming

Coke deposition during *n*-butane steam reforming was examined in a thermogravimetric apparatus using a feed mixture comprising diluted *n*-butane and steam. Both the 8.8 and 15.8% Ni samples supported on $MgAl_2O_4$, with and without 0.5% gold, were examined. The weight gain for these catalysts, operating at 500 °C and H_2O/C ratio of 0.7, are shown in Fig. 9. The 15.8% Ni catalyst exhibited poor resistance to coking under these conditions, with rapid coke deposition over the first 200 min, eventually leading to an overall weight gain exceeding 350 wt% at the end of a 16-h reaction period. Lowering the Ni content to 8.8% resulted in less carbon deposition.

Adding Au to these samples suppressed coke deposition, especially for the high-Ni sample, in which overall coke deposition at the end of the reaction was reduced by at least 60%. Similar experiments were repeated at 450 and 550 °C, and the cumulative amounts of coke deposited over the course of the

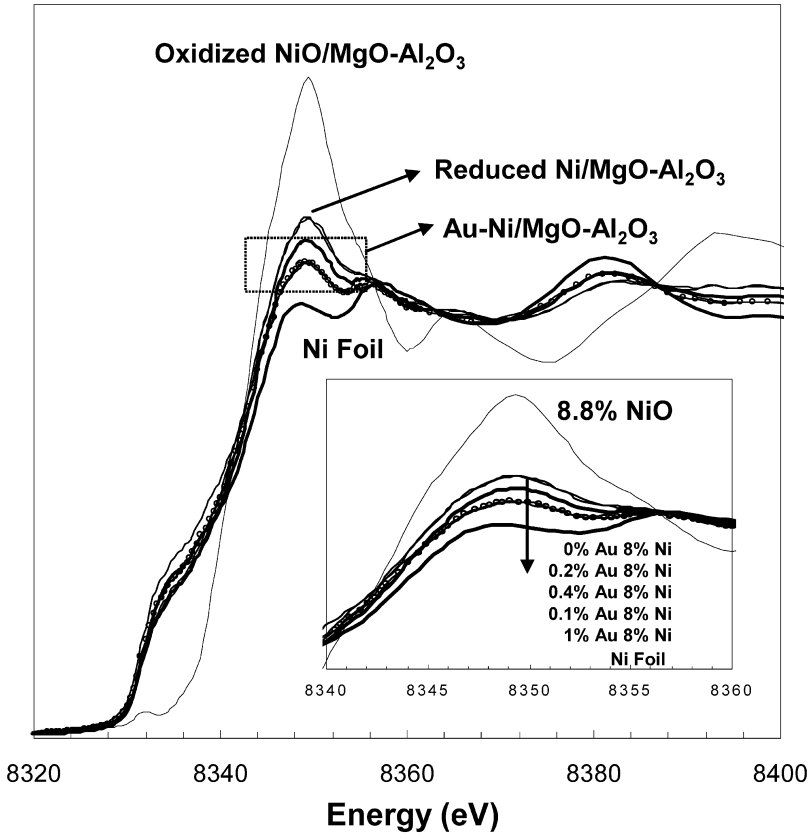

Fig. 7. Normalized XANES spectra at Ni K edge of Ni and Au–Ni/$MgAl_2O_4$ after reduction at 500 °C. A spectrum of Ni foil is included as reference.

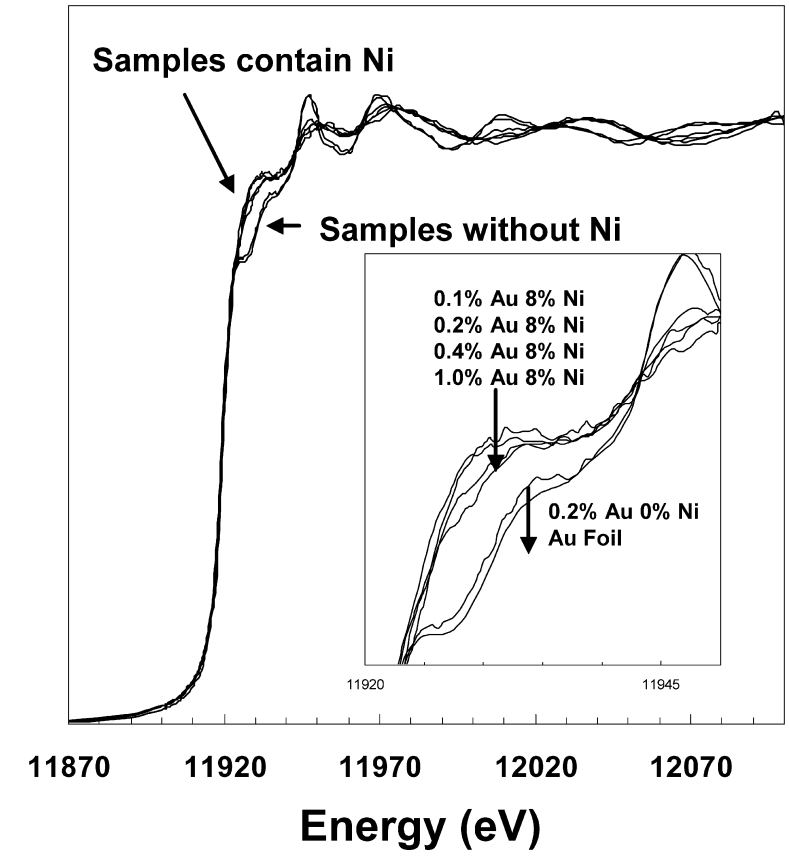

Fig. 8. Normalized XANES spectra at Au L_{III} edge of Au–8.8% Ni/$MgAl_2O_4$ after reduction at 500 °C. A spectrum of Au foil is included as reference.

Table 4
Effect of reaction temperature on the initial coke deposition rate and cumulative amount of coke deposited after 500 min *n*-butane steam reforming reaction at S/C of 0.7

SR temperature (°C)	Initial coking rate (wt%/min)			Coke deposition (wt%)		
	450	500	550	450	500	550
8.8% Ni/MgO–Al_2Q_3	21.2	64.5	43.0	141.9	148.4	121.1
0.5% Au–8.8% Ni/MgO–Al_2O_3	6.1	41.3	48.0	114.3	122.4	108.2
15.8% Ni/MgO–Al_2O_3	156.5	151.5	113.5	514.8	356.7	219.7
0.5% Au–15.8% Ni/MgO–Al_2O_3	45.3	64.4	47.0	192.0	181.8	131.4

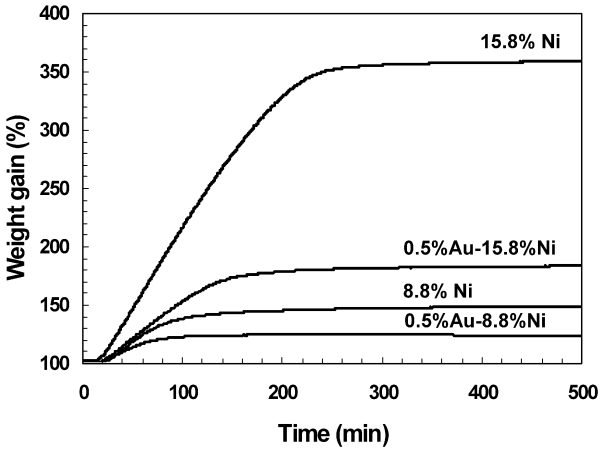

Fig. 9. TGA profile recorded during *n*-butane steam reforming over Ni–Au/$MgAl_2O_4$ using S/C of 0.7 at 500 °C. Feed: 2.1% H_2O, 0.75% *n*-butane, balance He.

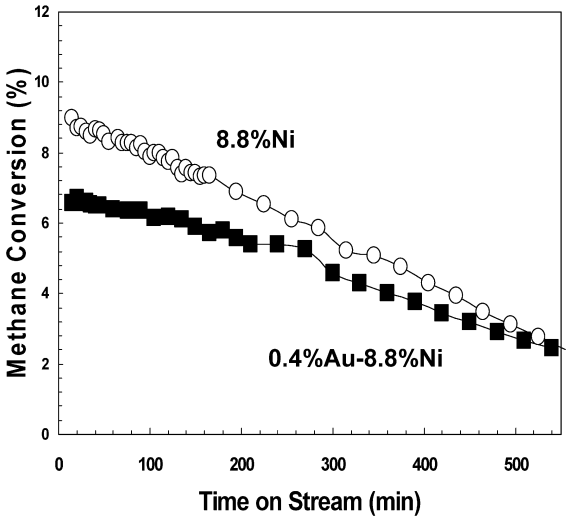

Fig. 10. Methane steam reforming activity over 8.8% Ni/$MgAl_2O_4$ (○) and 0.4% Au–8.8% Ni/$MgAl_2O_4$ (■). Conditions: 550 °C, $H_2O/CH_4/H_2$ = 4.5/4.5/1, 3.3×10^6 cc/(h g).

16-h steam-reforming period are tabulated in Table 4. The initial coking rates, derived from fitting the linear portion of the TG profile at the beginning of the reaction, are also listed in Table 4. Total coke deposition was the lowest for all samples at 550 °C, whereas initial carbon deposition was generally the highest at 500 °C. Comparing the unpromoted Ni and bimetallic Au–Ni samples shows that adding Au inhibited coking most effectively at 450 °C and to a decreasing extent with increasing temperature.

3.6. Methane steam reforming

Methane steam reforming was carried out with the 8.8% Ni/$MgAl_2O_4$ and 0.4% Au–8.8% Ni/$MgAl_2O_4$ catalyst at 550 °C, $H_2O/CH_4 = 1$, and $H_2O/H_2 = 4.5$. A space velocity of 3.3×10^6 cc/(h g) was used. H_2 was added to prevent nickel oxidation. Fig. 10 compares the time-on-stream activity of the two catalysts. Both catalysts showed deactivation with time on stream over the 500-min duration of the experiment; however, the apparent deactivation rate was lower for the Au-promoted catalyst. Our experience has shown that initial catalyst deactivation may be a combination of nickel sintering in the presence of steam as well as a result of carbon deposition. Thus the slower deactivation rate with the Au–Ni sample cannot be unequivocally attributed to improved stability to carbon formation, although the low S/C ratio used would favor that assessment. Initial methane conversion for the 0.4% Au–8.8% Ni/$MgAl_2O_4$ catalyst was reduced by approximately 20% compared with the 8.8% Ni/$MgAl_2O_4$ catalyst.

4. Discussion

The characterization studies described above (H_2 chemisorption, N_2O TPD, EXAFS, and XANES) all provide consistent evidence of a significant interaction between gold atoms and reduced Ni crystallites supported on $MgAl_2O_4$. The EXAFS measurements were especially instructive in providing information about the bimetallic alloy structure. With an oxidized sample, no interaction between the metallic Au atom and Ni oxide was observed. The Au atoms remained in a reduced state as aggregated metallic Au clusters with a coordination number close to 12. At these high average coordination numbers, the EXAFS data were unable to provide further information on Au cluster size, although the clusters likely were at least 30 Å in diameter. Thus, when Ni is in an oxidized state, it appears that individual Au atoms interact only with other Au atoms and not with NiO. On reduction, Au appears to disperse and preferentially migrate to the surface of the nickel clusters, as shown in the analysis of the Au L_{III}-edge EXAFS data in Fig. 5.

Analysis of the EXAFS data provides quantitative information on the Au–Ni bonding and coordination. On the reduced Ni sample with the lowest Au loading (0.1 wt%), the only interaction detected was the Au–Ni hetero-atomic bond. The average Au–Ni coordination was determined to be 5.3, consistent with the previously reported finding [18] that Au is located on the surface, whereas the full coordination of each Au atom in the

bulk Ni crystal (fcc) structure would be 12. There was no indication of any Au–Au bonding in this sample. A plausible model, consistent with these data, is that discrete Au atoms decorate the various exposed Ni crystallographic planes. With increasing Au loading, evidence of Au–Au interactions from the traces in the region of 2.4–3.4 Å was seen (Fig. 5). The Au–Au interactions arose either from formation of segregated Au clusters formed on the $MgAl_2O_4$ support or from interaction of multiple Au atoms on the Ni surface. Lack of a Ni–Au contribution in the Ni K-edge EXAFS spectra confirms that the Au atoms were not soluble in the bulk Ni crystal, even at the higher Au loadings. Holmblad et al. [20] showed that Au remains as a surface alloy up to temperatures of 577–627 °C, above which there is evidence of Au dissolution into the bulk. This temperature is well above that used in our measurements. Our results on the effect of increasing Au concentration are in agreement with findings of a Monte Carlo investigation by Fan and Gong of Au on a Ni(110) surface [21]. In that study, increasing the Au concentration above a surface coverage of 0.4 monolayer caused the Au–Ni surface alloy to undergo a phase transition in which the surface Au atoms nucleated to form a separate phase on the Ni.

The XANES data indicate that Au modified the electronic properties of Ni. Changes in the white line intensities (Figs. 7 and 8) of both the Ni K edge and Au L_{III} edge on the bimetallic samples reflect the modification of local electronic density on alloy formation. The increase in Au white line intensity accompanied by a concurrent decrease in the Ni white line intensity indicates that Ni acts as an electron acceptor in the alloy, withdrawing electron density from the neighboring Au atoms. Density functional calculations have suggested an increase in the dissociation barrier for CH_4 activation on Au-modified Ni(111) surfaces due to shifting in the local electron density of the Ni *d*-band in the presence of Au [22].

The adsorption properties of Ni changed significantly after the addition of Au, as shown in both the H_2 chemisorption and N_2O TPD studies. The suppression of H_2 chemisorption cannot be explained simply by geometric site blocking. Based on the measured hydrogen uptake, it appears that a single surface atom of Au can reduce the hydrogen chemisorption of as many as 6–9 nickel atoms. This finding is consistent with a previous study by Holmblad et al. over a Ni(111) single crystal doped with a sub-monolayer of Au [20] that found that desorption energies of CO and deuterium, determined from TPD spectra, decreased by approximately 25–30 kJ/mol when Au was loaded onto Ni(111) at a coverage of 0.7 monolayer. As a result, saturation coverage was reduced for both species. Similarly, the addition of Au suppressed N_2O chemisorption over the $Ni/MgAl_2O_4$ catalysts. Irreversible adsorption, resulting in decomposition of N_2O to produce N_2 and generate a surface nickel oxide, was drastically reduced on the Au-modified samples. This system is complicated due to the nondissociative adsorption of N_2O, which occurs in parallel with the dissociative pathway. This latter mode of adsorption appears to be rather complex and not easily explained, and further work is needed to elucidate this aspect of Ni–N_2O surface chemistry. However, the effect of Au in retarding the dissociative chemisorption of N_2O is clear.

Thermogravimetric studies of *n*-butane steam reforming were carried out at low S/C conditions aimed at facilitating coke deposition on the catalyst. Under these conditions, in the presence of diluted feed, we confirmed that adding 0.5 wt% Au to the $Ni/MgAl_2O_4$ catalysts reduced both the amount of carbon formed and the rate of carbon deposition, consistent with previously reported studies [6,14]. However, we note that when the reaction temperature was increased from 450 to 550 °C, the gold promoter was decreasingly effective in reducing carbon formation, as reflected in a lower fractional reduction in both the rate of carbon formation and total carbon deposited.

The methane steam-reforming experiments showed that adding Au resulted in a modest decrease in catalyst activity. This decrease was much less than what would be predicted based on the H_2 chemisorption and N_2O TPD characterization results. Because it has been shown that the step and edge sites are the most active for steam reforming, and are also the sites preferentially occupied by Au [6], it is not surprising that Au had an effect on reducing activity even though Au site occupation was less effective with increasing temperature. Along with the decrease in initial activity with the Au-promoted $Ni/MgAl_2O_4$, the deactivation profiles were also different. The 0.4% Au-promoted sample showed a less-steep deactivation profile, so that the two conversion curves appear to cross at about 10 h on stream. This suggests that the Au-containing sample had somewhat improved stability toward deactivation. Although it is tempting to ascribe these differences to the role of Au in retarding carbon formation, care must be taken with this assessment. Deactivation from metal sintering can also contribute to the observed decrease in catalyst activity. Because of the small amount of catalyst used in these tests, its characterization for carbon content or reduced metal surface area proved difficult and unreliable. Thus, our most relevant data on the ability of Au promotion to reduce the carbon-forming tendency with Ni catalysts remain those from the butane-reforming TGA studies.

5. Conclusion

The present study was undertaken to characterize the interaction between Au and Ni in a series of $Au–Ni/MgAl_2O_4$ catalysts. Au is known to form a surface alloy with Ni, and Au addition has been shown to reduce graphitic carbon formation during butane steam reforming [6]. Significant reductions in H_2 chemisorption and dissociative N_2O adsorption were observed after Au was added to $Ni/MgAl_2O_4$. These reductions were significantly greater than could be accounted for by a simple site blockage by Au and are more consistent with an electronic effect in which Au affects the adsorption properties of several adjacent Ni sites. Au L_{III}-edge EXAFS measurements showed a significant Au–Ni nearest-neighbor interaction when the Ni component was in the reduced state, but there appeared to be no interaction between Au and oxidized Ni. At the lowest Au loading (0.1 wt%), only Ni nearest neighbors were detected. At higher Au concentrations, there was evidence of both Au–Ni

and Au–Au bonds. XANES analysis of the Au–Ni/$MgAl_2O_4$ catalysts revealed changes in both the Ni K-edge and Au L_{III}-edge white line intensities, indicative of transfer of electronic charge from Au to Ni as a result of surface alloy formation.

From TGA measurements, the addition of Au was found to retard carbon deposition during *n*-butane steam reforming over the temperature range of 450–550 °C, consistent with previously reported results [14]. However, carbon formation was not totally suppressed, and with increasing temperature, the effect of Au addition decreased. Addition of 0.4 wt% Au to 8.8% Ni/$MgAl_2O_4$ showed a small decrease in catalyst activity and a small increase in catalyst stability for methane steam reforming at 550 °C. The activity decline was significantly less than would be predicted based on the H_2 chemisorption and N_2O TPD measurements. This suggests that the effect of Au was substantially more pronounced at the near-ambient temperatures used for catalyst characterization than at the higher temperatures used in steam reforming.

Acknowledgments

Support of this work by the US Department of Energy, Office of Fossil Energy, through the Solid State Energy Conversion Alliance (SECA) program is gratefully acknowledged. This work was performed in the Environmental Molecular Sciences Laboratory, a national scientific user facility sponsored by the U.S. Department of Energy's Office of Biological and Environmental Research, located at the Pacific Northwest National Laboratory in Richland, WA. The authors thank Professor J. Nørskov for helpful and informative discussions and Aritomo Yamaguchi for discussions of the EXAFS data.

References

[1] J.R. Rostrup-Nielsen, Steam Reforming Catalysts, Teknisk Forlag, Denmark, 1975.
[2] M.V. Twigg, Catalyst Handbook, second ed., Manson, London, 1994.
[3] Gas Making and Natural Gas, BP Trading, London, 1972.
[4] J. Sehested, Catal. Today 111 (2006) 103.
[5] J.R. Rostrup-Nielsen, in: J.R. Anderson, M. Boudart (Eds.), Catalysis, Science, and Technology, vol. 5, Springer-Verlag, Berlin, 1984, chap. 1.
[6] H.S. Bengaard, J.K. Nørskov, J. Sehested, B.S. Clausen, L.P. Nielsen, A.M. Molenbroek, J.R. Rostrup-Nielsen, J. Catal. 209 (2002) 365.
[7] D.L. Trimm, Catal. Today 37 (1997) 233.
[8] J. Wei, E. Iglesia, J. Catal. 224 (2004) 370.
[9] J.R. Rostrup-Nielsen, J. Catal. 85 (1984) 31.
[10] H.C. Dibbern, P. Olesen, J.R. Rostrup-Nielsen, P.B. Tottrup, Hydrocarbon Process. 65 (1986) 71.
[11] J.R. Rostrup-Nielsen, Natural Gas Conversion II, in: H.E. Curry-Hyde, R.F. Howe (Eds.), Stud. Surf. Sci. Catal., vol. 81, Elsevier, Amsterdam, 1994, p. 25.
[12] T.B. Massalski (Ed.), Binary Alloy Phase Diagrams, Am. Soc. Metals, Metals Park, OH, 1987.
[13] L. Pleth Nielsen, F. Besenbacher, I. Stensgaard, E. Lægsgaard, Phys. Rev. Lett. 71 (1993) 754.
[14] F. Besenbacher, I. Chorkendorff, B.S. Clausen, B. Hammer, A.M. Molenbroek, J.K. Norskøv, I. Stensgaard, Science 279 (1998) 1913.
[15] G. Yuan, J.L. Lopez, C. Loius, L. Delannoy, M.A. Keane, Catal. Commun. 6 (2005) 555.
[16] L. Yan, T. Ren, X. Wang, D. Ji, J. Suo, Appl. Catal. B Environ. 45 (2003) 85.
[17] F. Gonçalver, G.E. Marnellos, E.A. Efthimiadis, J.L. Figueiredo, React. Kinet. Catal. Lett. 80 (2003) 153.
[18] A.M. Molenbroek, J.K. Norskøv, B.S. Clausen, J. Phys. Chem. B 105 (2001) 5450.
[19] R. Puddephatt, The Chemistry of Gold, Elsevier, New York, 1978.
[20] P.M. Holmblad, J. Hvolbæk Larsen, I. Chorkendorff, J. Chem. Phys. 104 (1996) 7289.
[21] W. Fan, X.G. Gong, Surf. Sci. 562 (2004) 219.
[22] P. Kratzer, B. Hammer, J.K. Norskøv, J. Chem. Phys. 105 (1996) 5595.